THE FIRST SELF-PRIMING AND BI-DIRECTIONAL VALVE-LESS DIFFUSER MICROPUMP FOR BOTH LIQUID AND GAS

Wouter van der Wijngaart, Helene Andersson, Peter Enoksson,
Kjell Noren and Göran Stemme

Department of Signals, Sensors and Systems
Royal Institute of Technology, S-10044 Stockholm, Sweden

Keywords: micropumps, diffuser pumps, bi-directional pumping, self-priming, cavitation

ABSTRACT

A new micropump design was fabricated to make a qualitative study on the reliability of micro diffuser pumps. A novel two-level pump chamber geometry enables both gas and liquid pumping. The micropumps are fully self-priming and insensitive to cavitation and gas bubbles in the liquid. Changing the driving frequency enables bi-directional pumping for both liquid and gas, *i.e.* both forward and reverse pumping. The pumps consist of a silicon-glass stack and are fabricated with a new process involving three sequential DRIE (Deep Reactive Ion Etching) steps. A new and simple melt-on method for conveniently fixing external tubes to the device was developed. Design, fabrication and first experimental results are described and discussed in this paper.

INTRODUCTION

Displacement micropumps can be divided into two groups depending on the type of fluid directing element: pumps with passive check valves [1-4] and valve-less pumps [5-8]. Both gas pumping and liquid pumping has been shown to have good pressure-flow characteristics.
An important requirement for liquid pumping and a challenge for micropumps is pump *reliability*. Reliability involves a number of specific features.
One such feature is self-filling. The pump must be able to create an under-pressure, sucking liquid towards the pump inlet, and to fill without trapping of gas pockets. Reliability also involves pumping during a longer time period, during which small particles or gas bubbles dissolved in the pumped liquid should not degrade device performance. Particle sensitivity is an inherent problem for check valve pumps, in which the moving valves tend to clog or may suffer from fatigue and failure. Diffuser pumps do not suffer from these restrictions since they have no moving parts and/or small flow channel geometry. However, diffuser pumps presented earlier [5] are very sensitive to gas bubbles and cavitation (*i.e.* vapour formation resulting from a liquid pressure drop below the vapour pressure). These pumps require an extensive priming procedure, making them unreliable for practical applications.
The pump design presented in this paper solves all of the above mentioned problems. An exploded view of the design is shown in figure 1.

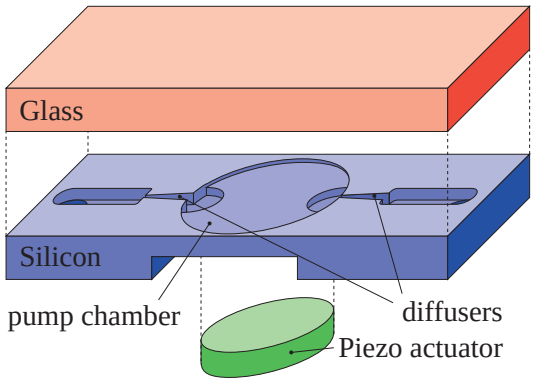

***Figure 1**. Exploded view of the pump structure.*

RELIABLE LIQUID PUMPING WITH MICRO DIFFUSER PUMPS

An under-pressure at the pump inlet, required for self-filling, can be achieved if the pump has both gas and liquid pumping properties. Good gas pumping can be achieved with a high pump compression ratio, *i.e.* a high pump stroke over chamber dead volume ratio. This results in a high pressure change inside the pump chamber during one pump cycle and thus better performance.
A high compression ratio is also the strategy to tackle gas bubble problems during liquid pumping. Gas bubbles in diffuser pumps introduce a specific problem when they reach a certain size. Due to surface tension forces, bubbles tend to “stick” to the pumps internal surface, especially in regions with low flow velocity. The compressible gas in the bubble then functions as a buffer for the pump chamber expansion and contraction, *i.e.* the liquid flow through the diffusers drops, prohibiting any further pump action. Gas bubbles originate both from gas dissolved in the liquid and from cavitation. The latter occurs in the pump at places with

high flow velocities and/or rapid changes in the static pressure. For micro diffuser pump designs this occurs respectively at the diffuser necks and at the centre of the pump diaphragm.

A high compression ratio affects the reliability of liquid pumping in several ways. First, the probability for a certain liquid volume to remain inside the pump chamber over a longer time period decreases. Therefore, the small gas bubbles present in this volume do not have the opportunity to get stuck or form bigger gas bubbles. Second, if the change in chamber volume during a pump stroke is higher than the buffer action of the present gas bubbles, the pumping action becomes bubble-tolerant. Third, a large compression ratio results in high flow velocities inside the pump chamber. A high flow velocity keeps the gas bubbles in motion rather than sticking at certain positions.

An increase of the compression ratio can be obtained by lowering the chamber dead volume, *i.e.* a shallow pump chamber, combined with a large diaphragm amplitude. A shallow pump chamber can easily be created using proper fabrication parameters. To obtain a large diaphragm amplitude, a qualitative study of a diaphragm-piezodisc bimorph was performed.

Modelling the pump diaphragm-piezodisc bimorph implemented in our pump design is not straightforward because the pump diaphragm itself is clamped at its circumference only on one side. There is also a difference in diameter between the piezodisc and the pump diaphragm. A full model of this construction would require Finite Element Analysis. We opted for a simplified model, described in [10] and illustrated in figure 2. The model consists of a stack made up of a diaphragm and a piezodisc with equal diameter and a guidance as border condition.

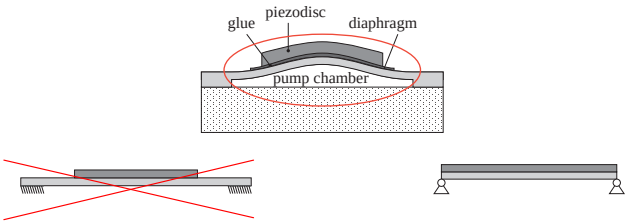

***Figure 2**. Modelling of the pump actuation using a simplified model.*

The analytical formula for the diaphragm deformation can then be written as

$$w(r) = \frac{R^2 - r^2}{h_p^2\left[3\left(1-\alpha^2\eta\right)^2 - 4\left(1+\alpha\eta\right)\left(1+\alpha^2\eta\right)\right]} \cdot \left[3d_{33}(1+\alpha)\alpha\eta\Phi_0\right]$$

where $\eta = s_{11}^E \cdot E \cdot \left(1-\nu_p^2\right)/\left(1-\nu_m^2\right)$

R = the overall radius

h_p = the piezodisc thickness

α = the ratio of the diaphragm thickness to the piezodisc thickness

Φ_0 = the voltage over the piezodisc

ν = Poisson's ratio

d_{33} = the piezoelectric charge constant

s_{11} = the elastic compliance

E = the Young's modulus of the diaphragm material.

This formula describes the static deflection of the bimorph structure under a certain driving voltage. It does *not* describe the dynamic behaviour of the pump diaphragm, *nor* does it take into account any fluid forces from inside the pump chamber. Nevertheless, it relays information about the diaphragm and piezodisc thickness and the preferred diaphragm material. A contour plot of the calculated maximal centre deflection of the diaphragm-piezodisc bimorph as a function of the piezodisc thickness and the diaphragm thickness is shown in figure 3. When using discrete glued-on piezodisc elements with a standard thickness, this model indicates that an optimal silicon diaphragm thickness results in a 20% higher deflection than an optimal glass diaphragm thickness. In general, thin and stiff diaphragms are advantageous when the piezodisc thickness is fixed. For a 0.1 mm thick piezodisc, a silicon diaphragm thickness of 34 µm is predicted to be optimal.

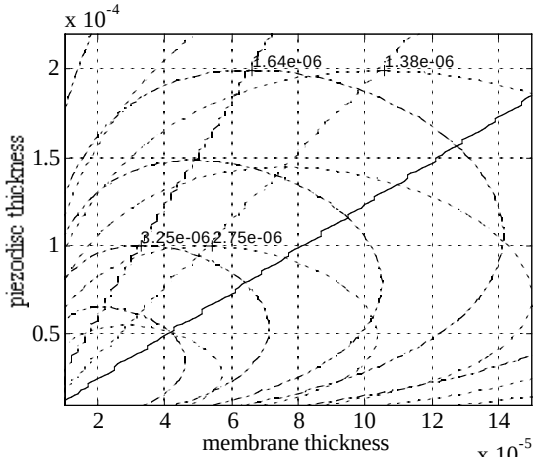

***Figure 3**. Contour plot of the calculated maximal centre deflection of the diaphragm-piezodisc bimorph as a function of the piezodisc thickness and the diaphragm thickness. The curves show the diaphragm- piezodisc thickness combinations with equal diaphragm deflections. The dash-dotted curves show the result for silicon as the diaphragm material. The dotted curves show the result for glass (Pyrex 7740) diaphragms. The straight dash-dotted and dotted lines connect the respective points with maximum centre deflection when a fixed piezodisc thickness is chosen. The numeric values indicate the diaphragm deflection (in µm) at the chosen parameter combination. The straight full line marks the border between thickness combinations that predict higher deflection (upper left part of the graph) for silicon than for glass as the diaphragm material.*

The thin bimorph and high compression ratio result in a high fluid displacement inside the pump chamber during

one pump stroke. The resulting flow patterns inside the pump chamber are discussed in a later section.
The thin diaphragm also allows a wide driving frequency range. Older pump versions were limited to the resonance driving frequency because the stiff diaphragm did not allow satisfactory diaphragm amplitudes at non-resonance frequencies. This reveals fundamental new diffuser behaviour, allowing both forward and reverse pumping.

FABRICATION

The pumps are fabricated using a new fabrication sequence, shown in figure 5, allowing three sequential DRIE steps on the same surface.
Prior to any etching, three masks are deposited and patterned on the silicon: an oxide mask (a), an aluminum mask (b) and a photoresist mask (c). In a first etch, fluid connections are created at the in- and outlet (d). The resist mask is removed and in a second etch the deep diffusers are formed (e). The shallow pump chamber is created during a third etch after removal of the aluminum mask (f). After the oxide is removed, the silicon wafer is anodically bonded to a Pyrex wafer (g). In a last DRIE step, the pump diaphragm is thinned down (timed etch stop) and in-and outlet fluid connectors are formed on the back side of the silicon (h). Typical pump dimensions are given in figure 6. Limiting the diffuser depth to 30 µm allowed an increased mask design freedom. The region around the diffuser inlet/outlet, a region where typically high flow velocities occur [diffuser simulations], was etched deep to avoid any influence on the diffuser functionality.
After dicing the wafer, a 4 mm diameter, 0.1 mm thick piezo disc is glued and contacted to the pump

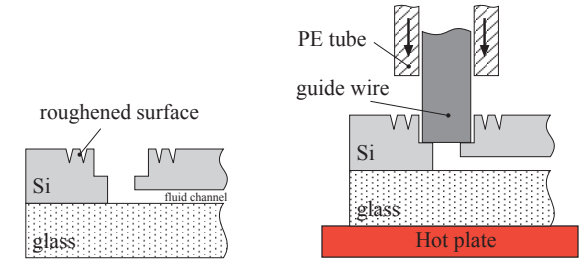

1. Chip with roughened surface

2. A guide wire ensures proper alignment of tube and fluid openings

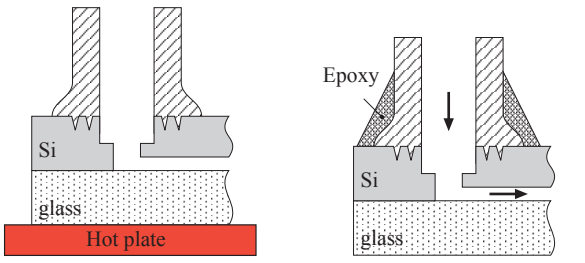

3. A brief melting of the PE tube ensures perfect sealing.

4. Epoxy gives additional strength.

***Figure 4**. Fluid connectors are applied using a new melt-on method.*

a Grow and pattern oxide mask.

b. Sputter and pattern aluminum mask.

c. Apply photoresist mask.

d. First DRIE (Deep Reactive Ion Etch).

e. Remove photoresist ; second DRIE.

f. Remove aluminum ; third DRIE.

g. Remove oxide ; anodic bonding.

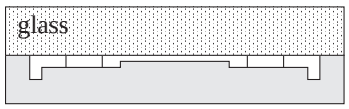

h. Thin down diaphragm and open up fluid connectors with another DRIE.

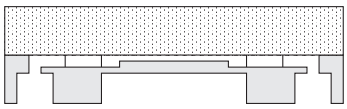

***Figure 5**. Schematic of the fabrication process.*

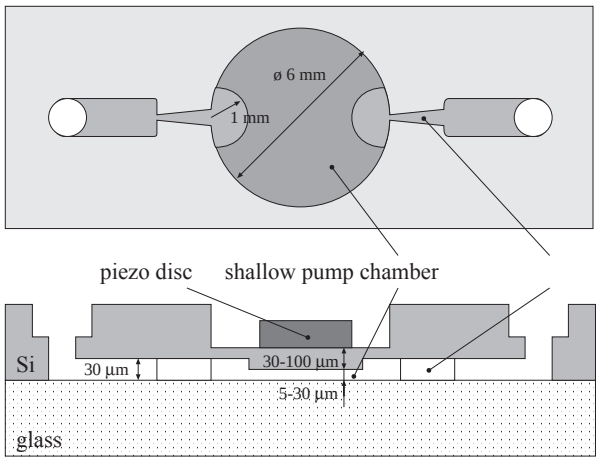

***Figure 6**. Schematic of a complete pump with typical dimensions. The diffuser neck is square and measures 30 µm deep and wide. The shallow chamber depth varies between 5 and 30 µm. The pump chamber diameter measures 6 mm in all designs.*

diaphragm. External polyethylene (PE) tubes are used as fluid connectors and are fixed to the chip in a multi-step procedure as schematically shown in figure 3. A mask-defined silicon surface roughening was performed around the fluid openings by DRIE to ensure good adhesion of the PE tubes. A guide wire is used to align the PE tube with the fluid openings on the chip. The silicon-glass stack is shortly heated to generate a local melting of the PE tube onto the chip. To give additional strength to the assembly, the interface between the chip and the PE tubes is covered with epoxy glue.

EXPERIMENTS AND RESULTS

The pumps were designed for qualitative investigation of pump reliability and gas bubble tolerance. The small diffuser size (depth < 30 µm) enabled a larger geometrical design freedom, but resulted in poorer (quantitative) pressure-flow characteristics than presented in earlier papers [5]. A full investigation of different pump designs has not yet been performed. This paper focuses rather on qualitative than on quantitative results.

For pump pressure measurements, the pump inlet was left open (atmospheric pressure) and the pump outlet was closed (zero flow). Pressure was then measured at the closed pump outlet. Measurements at the pump inlet (with a closed inlet and open outlet) show the same pressure performance, *i.e.* the pump suction capability at the pump inlet (outlet) equals the pump pressure capability at the outlet (inlet).

Flow was measured leaving the in- and outlet at atmospheric pressure. The liquid flow was measured through the speed of the liquid column. The gas flow was calculated from the speed of a small liquid drop in a tube connected to the in- or outlet.

For gas pumping measurements, an automated system was set up in which an optical diaphragm deflection measurement was used as feedback to keep a constant diaphragm amplitude. A schematic of the set-up is shown in figure 7.

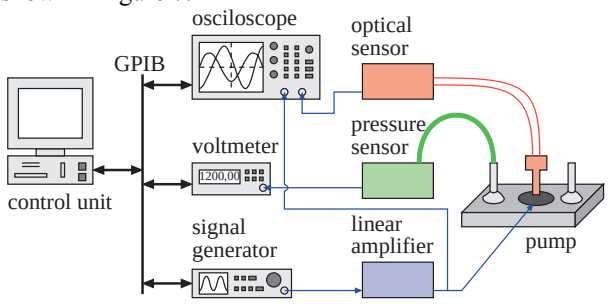

***Figure 7**. The automated measurement system.*

This feedback system reduces the influence of difficult controllable fabrication parameters such as the silicon diaphragm thickness and glue thickness. It also protects the pump from a too large (fatal) diaphragm deflection when a resonance mode is excited.

The pump performance values given below are preliminary results from the first investigated pumps. Figure 8 shows air pumping performance at different driving frequencies, maintaining a constant diaphragm deflection. The driving voltage of the piezo element was limited to 125 V so as not to destroy it. Therefore, at low driving frequencies, a large diaphragm amplitude could not be maintained. Figure 9 shows air pumping characteristics of another pump at different actuation voltages.

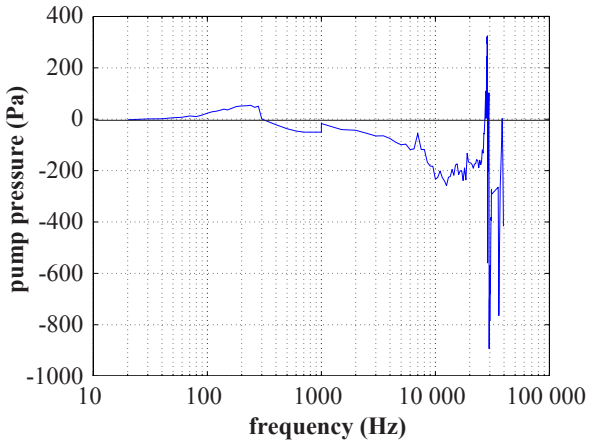

***Figure 8**. Pump pressure and diaphragm deflection for air pumping at different driving frequencies.*

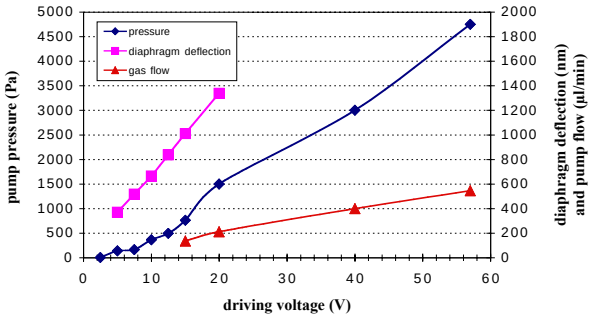

***Figure 9**. Pump pressure, flow and diaphragm deflection as a function of driving voltage for air pumping at a driving frequency of 33 kHz (close to resonance).*

An important observation is the bi-directional characteristics of the device. The delivered pump pressure changes from positive (forward) to negative (reverse) at approximately 400 Hz. The pressure remains negative until the first resonance peak at 27.5 kHz, where a positive pressure peak is observed. At the next resonance peak (29.5 kHz), reverse pumping occurs again. For higher driving frequencies, the diaphragm deflection tends to diminish. This is due to heating of the glue between the piezodisc and the pump diaphragm, resulting in temporarily failure of the glue. After the driving signal was switched off for a couple of minutes, allowing the structure to cool down, it was possible to drive the pump at these high driving

frequencies for a couple of seconds. Preliminary measurements in this high driving frequency range show a pump pressure in the kPa range.
It was observed that the flow directing capability of the diffusers is not only driving frequency dependent, but also amplitude dependent. A deeper understanding of the dynamic behaviour of the diffuser elements is still lacking.
Figure 10 shows the pump pressure and diaphragm deflection during water pumping with different driving frequencies. The liquid inside the pump chamber dampens the diaphragm amplitude, making a feedback system unnecessary. Here as well, both forward and reverse pumping could be obtained.

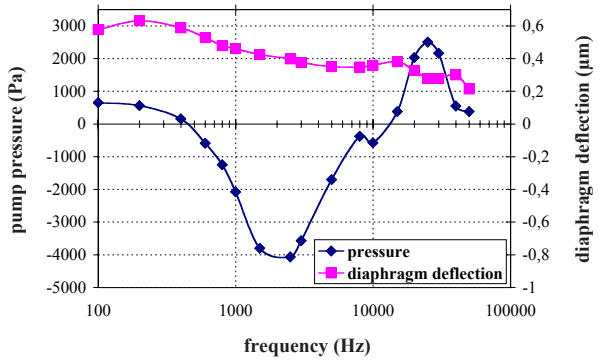

Figure 10. *Pressure and pump diaphragm deflection for water pumping at different driving frequencies. The driving amplitude is 100 V.*

Overall, the maximum obtained pressure range for air pumping was –4 kPa (reverse pumping) to 5 kPa (forward pumping) during this first test series. With 'forward' pumping we will refer to a net flow or pressure increase in the pumps positive diffuser direction, *i.e.* the direction in which the diffuser channel gets wider. 'Reverse' refers to the opposite direction. A maximum air flow of 545 µl/min was obtained.
The maximum obtained pressure range for pumping water is –4 kPa (reverse) to +5 kPa (forward). A maximum flow of –30 µl/min and +30 µl/min was measured, respectively.
Due to the non-optimised diffuser geometry, the pressures and flows reported above are much lower than the values presented in [A. Olsson]. However, the order of magnitude agrees with values extrapolated from earlier pump results [5,9]. Future versions will incorporate more optimal diffuser designs for enhanced flow-pressure performance.
Testing was also performed to determine whether gas pumping and liquid pumping could be performed subsequently with the same pump. A pump inlet was connected to a water bath using a tube. Gas pumping sucked the liquid to the pump inlet, after which immediate capillary filling occurred. The pump then successfully continued liquid pumping the water through its outlet.

DISCUSSION

A series of tests was performed with water as the pumped medium. Small particles were introduced into the liquid, so that the flow pattern inside the pump could be visually observed. Two important visual observations can be reported. First, vortex-like flow patterns occur in the pump chamber under all pump conditions. Secondly, cavitation is present under almost all pumping circumstances.
A number of different flow patterns observed inside the pump chamber are shown in figure 11.

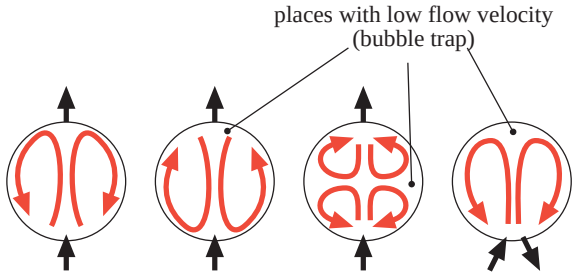

Figure 11. *Schematic drawing of some of the commonly observed flow patterns. The black arrows symbolise the diffusers. The grey arrows are the observed flow pattern. Some places inside the pump chamber with low flow velocity are indicated.*

The number of vortices and the direction in which they turn is dependent on driving frequency and diaphragm amplitude. Generally, the higher frequencies and/or diaphragm amplitudes result in a higher number of vortices and higher flow velocities.
The driving force behind these vortices could be that during pump chamber expansion, liquid is injected at high speed at the inlet- and outlet diffuser. These "fluid jets" transfer their kinetic energy to the surrounding liquid. This is shown schematically in figure 12.

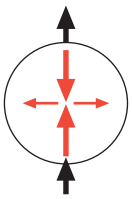

Figure 12*. Fluid jets at in-and outlet might cause vortex flow patterns.*

The flow patterns described above have a strong influence on gas bubble behaviour inside the pump chamber, and the presence of a gas bubble changes the flow pattern. For example, the buffering action of the bubbles results in a rapidly moving bubble surface and thus high liquid flow velocities around gas bubbles.
Cavitation occurs predominantly in the centre of the pump chamber. Higher diaphragm amplitudes and/or

higher driving frequencies enhance cavitation. The resulting small gas bubbles are transported in the liquid flow through the pump chamber. In some cases they are directly transported out of the pump chamber, where they slowly dissolve into the liquid. However some bubbles stick inside the pump chamber in places with a lower flow velocity (indicated in figure 11). These bubbles grow as more bubbles merge together. A high flow velocity inside the pump chamber ensures that large bubbles are torn into smaller parts that are almost immediately transported out of the pump chamber. In a wide frequency range, an equilibrium between bubble formation and bubble removal is established. During these conditions, the pump action is not limited by cavitation, making liquid degassing and pump priming unnecessary.

Under the above described conditions, the gas in the bubbles remains in the gas phase, and the surrounding liquid remains in the liquid phase. At certain pump frequencies and amplitudes, however, the fluid inside the pump chamber moves into the two-phase domain, *i.e.* the coexistence region where both liquid and vapour are present. This is illustrated in figure 13. In this state, the fluid pressure in the pump chamber remains constant and can not change (presuming the temperature remains constant). Any external energy supplied to the fluid, (*i.e.* coming from the piezoelectric actuator) is consumed as evaporation energy instead off pressure build-up.

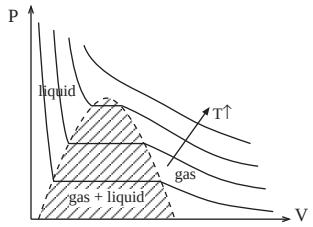

Figure 13*. The P-V relation for water. The arched area indicates the gas-liquid two-phase domain. The curves indicate isotherm lines. If the state of the pumped fluid lays in the arched area, the pressure can not be altered without a temperature change.*

Under these conditions, the pump performance drops almost to zero. The phase transition can be observed clearly in the pump. The gas bubbles present in the pump chamber become foggy, as small condensation drops are formed inside the bubbles. When the driving signal is not changed at this point, all the fluid inside the pump chamber moves into the coexistence region within a few seconds.

These phenomena only occur under specific circumstances though. A majority of driving signals result in reliable liquid pumping.

CONCLUSION

By varying design parameters it was shown that the ability of diffuser micropumps could be extended with several important key features: self-priming, bi-directional pumping and pumps with combined gas and liquid pumping. This enabled pumping of non-laboratory fluids like ordinary tap water without any priming procedure. It was also shown that changing the pumping frequency could control the direction of pumping. Pump pressures around 5 kPa were achieved in both directions for both liquid and gas pumping.

ACKNOWLEDGEMENTS

This research is sponsored by the Swedish National Board for Industrial and Technical Development through the competence centre SUMMIT (Surface and Micro structure Technology).

REFERENCES

[1] “A Self-priming and Bubble-tolerant Piezoelectric Silicon Micropump for Liquids and Gases", P. W. R. Linnemann, C.-D. Senfft, J.A. Ditterich, Proceedings MEMS '98, Heidelberg, p. 532-537

[2] "The VAMP - a new device for handling of liquids and gases", e. a. Stehr, 1996, Sensors and Actuators, vol A57, p. 153-157

[3] "A bidirectional silicon micropump", R. Zengerle e. a., 1995, Sensors and Actuators, vol A50, p. 81-86

[4] "A self-filling low-cost diaphragm micropump", J. D. K.-P. Kämper, W. Ehrfeld, S. Oberbeck, Proceedings MEMS '98, Heidelberg, vol p. 432-437

[5] "Micromachined flat-walled valve-less diffuser pumps", A. Olsson, P. Enoksson, G. Stemme and E. Stemme, 1997, IEEE Journal of Microelectromechanical Systems, vol 6, p. 161-166

[6] "Development of Bi-directional Valve-less Micropump for Liquid", A. K. S. Matsumoto, R. Maeda, Proceedings MEMS '99, Florida

[7] “Microdiffusers as dynamic passive valves for micropump applications”, T. Gerlach, 1998, Sensors and Actuators, vol A69, p. 181-191

[8] "The first valve-less diffuser gas pump", G. Stemme, E. Stemme and Anders Olsson, Proceedings MEMS '97, Nagoya

[9] "A Valve-less Planar Pump in Silicon", P. Enoksson, A. Olsson, G. Stemme and Erik Stemme, Proceedings Transducers '95 - Eurosensors IX, p. 305-B7

[10] "A Piezoelectric Capillary Injector", E. Stemme, and Larsson, 1973, IEEE Transactions on Electron Devices